TOTEM Note
10 February 2009

Acceptance of Protons in the TOTEM RP Detectors for LHC V6.500 Optics of Injection Energy (E = 450 GeV and $\beta^* = 11$ m)

Hubert Niewiadomski

Abstract

This note reports about the acceptance for elastically and diffractively scattered protons in the TOTEM Roman Pot detectors, placed 147 m and 220 m away from the IP5, for the LHC early collision optics with beams of injection energy: $E = 450$ GeV and $\beta^* = 11$ m. The results are based on thin lens proton tracking with the use of MADX and the aperture model of the machine.

The paper discusses also the behaviour of the optical functions at the Roman Pot locations as a function of the fractional proton momentum loss and reports its influence on the detection of diffractively scattered protons. The optical functions are obtained from proton tracks by means of multidimensional polynomial approximation.

1 Introduction

The TOTEM experiment [1, 2] is interested in detection of the intact protons scattered from the IP5. Such protons are measured by the near-beam telescopes, called Roman Pots (RP), placed at a distance of about 147 m and 220 m on both sides of IP5 (see [1] and [2]).

A proton produced in a diffractive interaction with the kinematic parameters[1] t, ϕ, ξ, x^*, y^*, passes a Roman Pot (RP) detector plane, placed at distance s from IP5, at a transverse position $(x(s), y(s))$ determined by the beam optics between the interaction point and the RP. The displacement $(x(s), y(s))$ is related to its transverse origin (x^*, y^*) and its momentum vector (expressed by the horizontal and vertical scattering angles Θ_x^* and Θ_y^* and by $\xi = \Delta p/p$) at the IP via the optical functions and the horizontal dispersion $D_x(s)$ of the machine:

$$\begin{aligned} x(s) &= \Delta x(s) + v_x(s) \cdot x^* + L_x(s) \cdot \Theta_x^* + \xi \cdot D_x(s) \\ y(s) &= v_y(s) \cdot y^* + L_y(s) \cdot \Theta_y^*. \end{aligned} \tag{1}$$

[1] The four momentum transfer squared is defined as $t = (E - E')^2 - (\vec{p} - \vec{p}')^2$, where the primed variables denote the quantities after the interaction. t can be also expressed [6] in terms of the scattering angle Θ, the initial momentum p, the proton mass m and the fractional momentum loss $\xi = \frac{p-p'}{p}$: $-t = -t_0 + 4p^2(1-\xi)\sin^2\frac{\Theta}{2}$ with the kinematic limit $-t_0 = 2\ p^2 + m^2\ \ \sqrt{1 + \frac{p^2(\xi^2-2\xi)}{p^2+m^2}} - 1\ \ + 2\xi p^2$.

The coefficients of Equation 1 depend upon the betatron function $\beta(s)$ and the phase advance $\Delta\mu(s)$ [3]. The functions $v(s)$ and $L(s)$ can be expressed as:

$$\begin{aligned} v(s) &= \sqrt{\frac{\beta(s)}{\beta^*}}\cos\Delta\mu(s) \\ L(s) &= \sqrt{\beta(s)\beta^*}\sin\Delta\mu(s) \\ \text{with}\quad \Delta\mu(s) &= \int_0^s \frac{1}{\beta(s')}ds'. \end{aligned} \tag{2}$$

The offset of the beam closed orbit with respect to the machine reference orbit is expressed by $\Delta x(s)$. In addition, the presence of the crossing angle at IP5 may introduce the beam tilt with respect to the reference orbit.

The Roman Pot detectors are placed at the transverse distance of $10 \times \sigma_{x,y} + 0.5\,\text{mm}$ from the beam centre, where $\sigma_{x,y}$ is the beam size at the location of the detector. The values of the effective lengths L_x and L_y (together with the beam size) determine the acceptance of the proton four momentum transfer $-t \approx p^2\,\Theta^{*2}$, where $p = 450\,\text{GeV}$ is the proton momentum and Θ^* is the scattering angle. Higher values of $L_{x,y}$ allow for detection of lower scattering angles and thus lower $|t|$ values. The value of the dispersion D_x determines the acceptance for $|\xi|$ for diffractively scattered protons. The magnifications v_x and v_y express the influence of the primary vertex position on the proton displacement at a given RP location.

The discussed early collision optics is characterised by the parameters given in Table 1.

Beam energy E	450 TeV
Lorentz γ	479.6
Normalised emittance ϵ_N	3.75 μm rad
β^*	11 m
Beam size $\sigma^*_{x,y}$	293.3 μm
Beam divergence $\sigma(\Theta^*_{x,y})$	26.7 μrad
Half crossing angle $\Theta_{x,c}$	46.97 μrad
Beam offset Δx^*	164.8 μm

Table 1: Beam parameters in IP5.

The collision optics at the energy of 450 GeV is characterised by generally thicker beams than in the case of the nominal LHC 7 TeV collision optics [4, 5]. Therefore, the Roman Pots need to be placed at the distance of about 1 cm from the beam centre, which results in very limited acceptance in the overlap area between the horizontal and vertical Roman Pots. The shape of the overlap between the horizontal and vertical detectors is presented in Figure 1. In addition thick beams imply reduced acceptance for high proton $|t|$ because of the losses in the machine apertures. The acceptance for elastically and diffractively scattered protons by the RP147 and RP220 stations is presented in the following sections.

The studies were carried out with the MADX [7] accelerator design programme. The

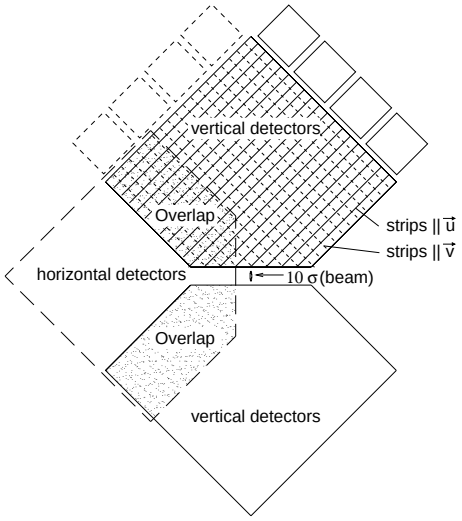

Figure 1: The overlap between the horizontal and vertical detectors.

optics parameters presented in Tables 1, 2 and 3 were computed with the Twiss Module, Equation (2) and standard accelerator optics formulae discussed in [3, 9], while the calculations of acceptance and chromaticity were based upon the Thin-Lens Tracking Module and the aperture database of the LHC [8]. The primary vertex position smearing was included in this study. However, for simplicity, beam divergence smearing was not applied. Although it may only slightly affect the acceptance study, it will be one of the limiting factors of proton reconstruction resolution. Since the LHC beams are very similar in the proximity of IP5, only LHC Beam 1 was analysed.

On the basis of the protons tracked through the lattice of the LHC, the multidimensional polynomial parameterisations of the transport were computed with the method discussed in detail in [9]. The approximations obtained were used to present the dependence of the optical functions upon the proton fractional momentum loss $\xi = \Delta p/p$. All the optics related calculations were performed within the optics software package of TOTEM.

2 Acceptance in RP 147

2.1 Elastic protons

The values of the optical functions and the positions of the RPs in the RP147 station are given in Table 2. The values of the effective lengths in horizontal and vertical projection are similar which results in the acceptance for elastically scattered protons in both horizontal and vertical RPs. However, the acceptance is not only limited by the effective lengths but also by machine apertures. Since the beams are larger when the machine is run at the energy of 450 GeV, the protons scattered at larger angles are absorbed by machine elements. This results in limited acceptance for higher $|t|$-values. The acceptance for elastically scattered protons in the RP147 station extends over the range of $0.02\,\mathrm{GeV}^2 <$

Magnification v_x	-1.88
Magnification v_y	-2.09
Effective length L_x	21.16 m
Effective length L_y	35.0 m
Dispersion D_x	-0.0788 m
Beam size σ_x	0.789 mm
Beam size σ_y	1.12 mm
Beam offset Δx	-2.18 mm
Beam tilt Θ_x	32.5 μrad
RP distance from beam centre x_{RP} $(10\,\sigma_x + 0.5\,\mathrm{mm})$	8.4 mm
RP distance from beam centre y_{RP} $(10\,\sigma_y + 0.5\,\mathrm{mm})$	11.7 mm

Table 2: Beam and RP parameters at 147 m from IP5 for $\xi = 0.0$.

$-t < 0.12\,\mathrm{GeV}^2$. The acceptance is much higher in case of the vertical RP (Figure 2, right) compared to the horizontal one (Figure 2, left). The elastically scattered protons visible in the horizontal RP can be considered as a background for diffractive proton detection which is performed primarily by the horizontal RPs.

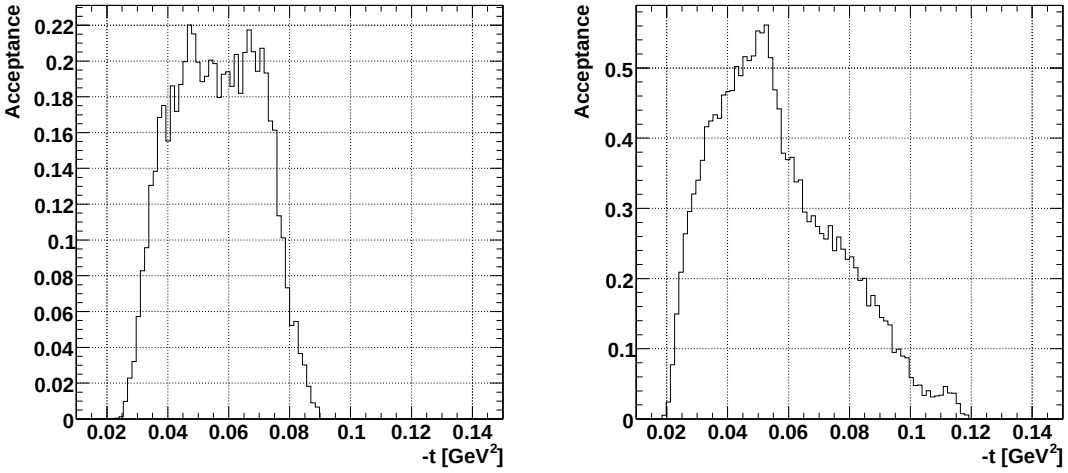

Figure 2: Acceptance of elastically scattered protons in the RP147 station. Left: Horizontal RP. Right: Vertical RP.

The acceptance for the overlapping region between the horizontal and vertical RP detectors of a given station is of particular interest for alignment procedures. Because of the shape of the silicon detectors placed in the RPs (see Figure 1 and also [1, 2]), the detectors may overlap if the sum of the displacements of the horizontal and vertical active edges, with respect to the centre of the reference orbit, is lower than about 2 cm. Because of large beams the area of the overlap is very limited, as presented in Figure 3 (right). The slight overlap is only due to the horizontal beam offset of -2.18 mm in RP147.

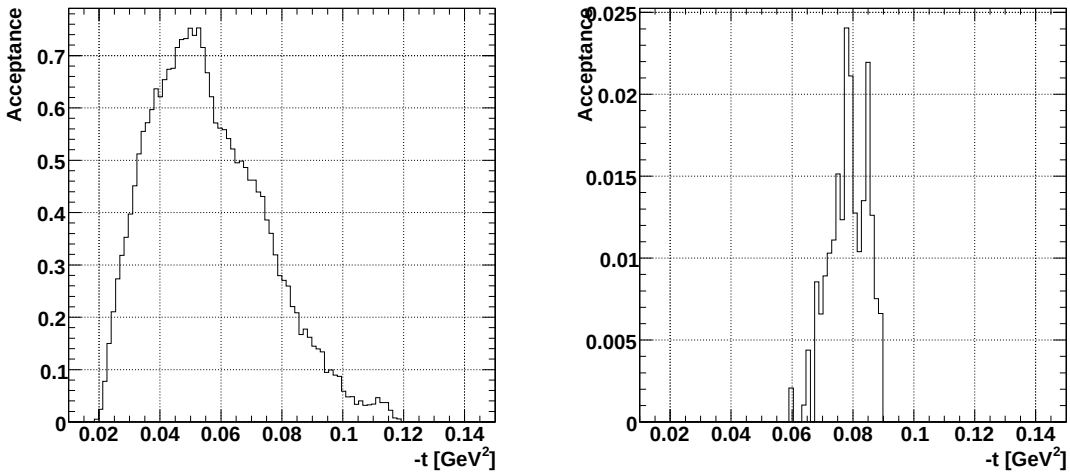

Figure 3: Acceptance of elastically scattered protons in the RP147 station. Left: Combined acceptance of the horizontal and vertical RPs. Right: Acceptance of the overlap of the horizontal and vertical RPs.

The combined acceptance of the vertical and horizontal pots is presented in Figure 3 (left).

2.2 Diffractive protons

The optical functions for the 450 GeV running scenario, obtained with MADX, exhibit a large dependence upon the fractional momentum loss of the proton.

The magnification values are presented in Figure 4. Although they will affect the

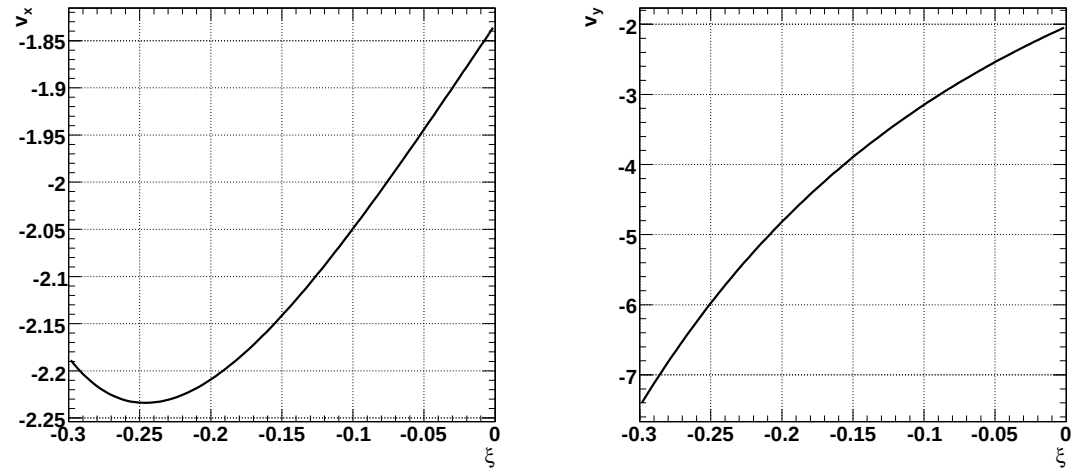

Figure 4: Magnification $v_x(\xi) = \partial x(s)/\partial x^*$ (left) and $v_y(\xi) = \partial y(s)/\partial y^*$ (right) at $s = 145\,\mathrm{m}$ from IP5 as a function of the fractional proton momentum loss ξ.

reconstruction resolution (beam size at IP5 is quite large), they are not affecting the acceptance in a significant way.

The dependence of the horizontal and vertical effective lengths upon ξ is shown in Figure 5. For $\xi = 0$, L_x and L_y are 21 m and 35 m, respectively. With increasing fractional

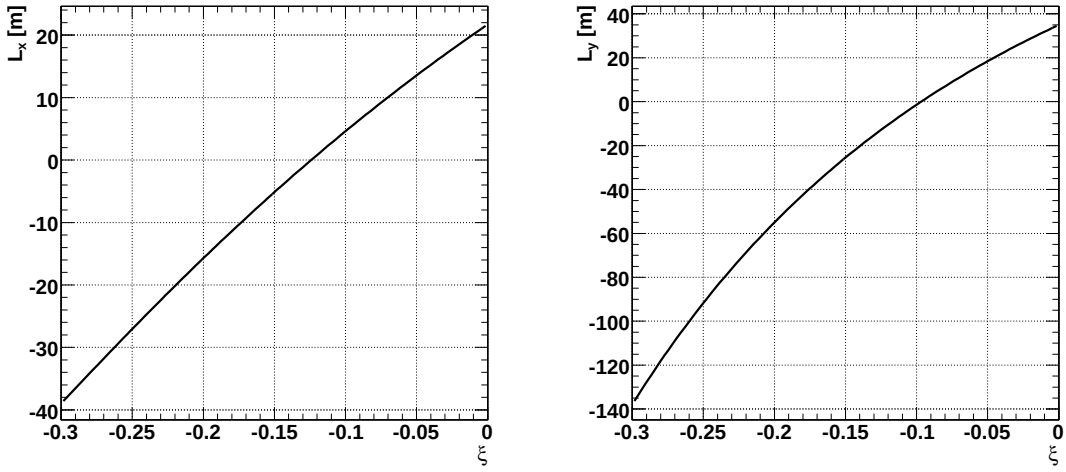

Figure 5: Effective lengths $L_x(\xi) = \partial x(s)/\partial\Theta_x^*$ (left) and $L_y(\xi) = \partial y(s)/\partial\Theta_y^*$ (right) at $s = 145\,\mathrm{m}$ from IP5 as a function of the fractional proton momentum loss ξ.

momentum loss they are reduced, reaching zero for $\xi = -0.125$ and $\xi = -0.09$, respectively. For such ξ the reconstruction of, respectively, the horizontal or vertical component of the proton scattering angle is not possible. For higher fractional momentum losses the effective lengths further decrease reaching high values with negative sign (especially L_y). This results in acceptance for the diffractively scattered protons not only in the horizontal RPs but also in the vertical ones.

The dispersion function, which is shown in Figure 6, also changes with ξ, which will affect the ξ-reconstruction resolution.

The acceptance for diffractively scattered protons in horizontal and vertical RPs is shown in Figure 7. For higher momentum losses ($-\xi > 0.1$) the protons are detected mainly in the horizontal detectors (Figure 7, left) due to the horizontal dispersion of the machine. In this case the acceptance reaches nearly 100 %. For lower $|\xi|$-values the acceptance is due to the proton scattering angles.

The vertical RPs also have acceptance for the diffractive protons, as it is visible in Figure 7 (right). The area of acceptance for $0.13 < -\xi < 0.25$ is caused by the large negative effective lengths caused by the machine chromaticity, as it was presented in Figure 5. For $0.05 < -\xi < 0.13$ there is no acceptance because the effective lengths are nearly 0, as it was already discussed. Finally, for $-\xi < 0.05$ the acceptance in the vertical RP is again due to the scattering angle, as in the case of the elastic scattering.

The combined acceptance of the horizontal and vertical detectors is presented in Fig-

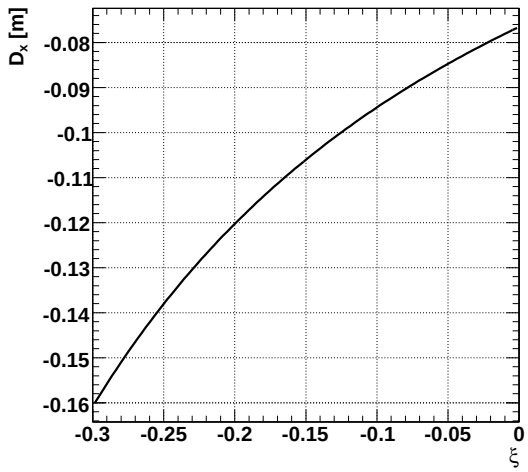

Figure 6: Dispersion $D_x(\xi) = \partial x(s)/\partial\xi$ at $s = 145\,\mathrm{m}$ from IP5 as a function of the fractional proton momentum loss ξ.

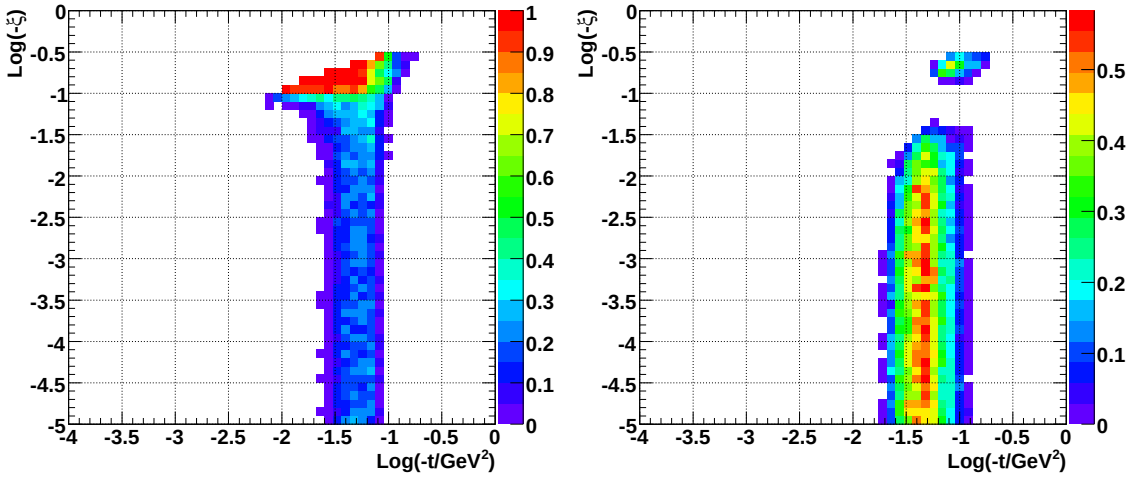

Figure 7: Acceptance in t and ξ for diffractively scattered protons in the RP147 station. Left: Horizontal RP. Right: Vertical RP.

ure 8 (left). The overlap between the horizontal and vertical RP is not large. However, even this small overlap acceptance, presented in Figure 8 (right), might be of use for alignment purposes.

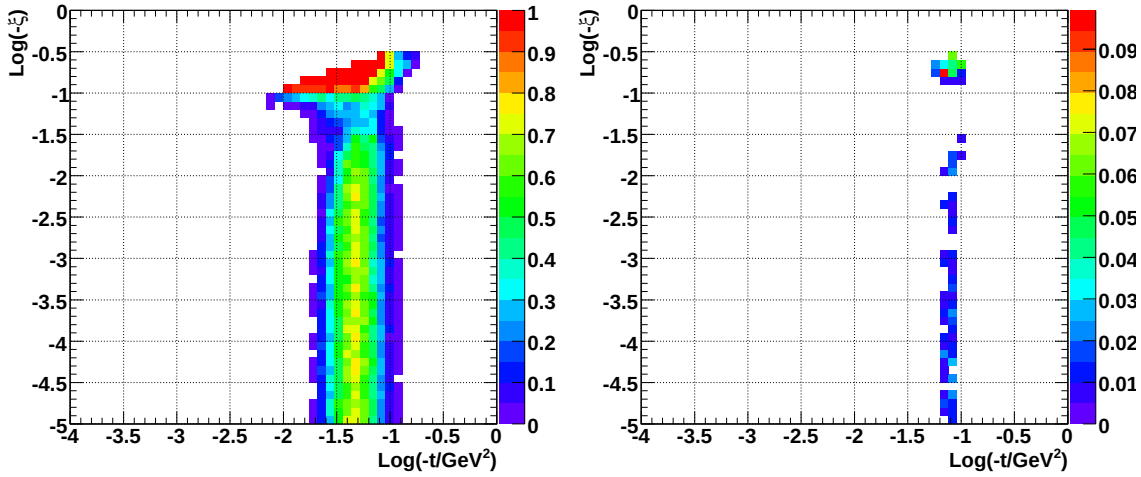

Figure 8: Acceptance in t and ξ for diffractively scattered protons in the RP147 station. Left: Combined acceptance in horizontal and vertical RPs. Right: Acceptance in the overlap area of the horizontal and vertical RPs.

3 Acceptance in RP 220

3.1 Elastic protons

The optics parameters and the RP positions in the RP220 station are given in Table 3. Since $L_x \approx 0$, the elastically scattered protons could only be detected by the vertical RPs.

Magnification v_x	-2.98
Magnification v_y	-3.47
Effective length L_x	4.72 m
Effective length L_y	19.44 m
Dispersion D_x	-0.084 m
Beam size σ_x	0.882 mm
Beam size σ_y	1.143 mm
Beam offset Δx	-1.166 mm
Beam tilt θ_x	66.8 μrad
RP distance from beam centre x_{RP} ($10\,\sigma_x + 0.5$ mm)	9.3 mm
RP distance from beam centre y_{RP} ($10\,\sigma_y + 0.5$ mm)	11.9 mm

Table 3: Values of optical functions at 220.5 m from IP5 for $\xi = 0.0$.

However, because of large beam sizes, such protons are nearly entirely lost in the machine apertures before reaching the RP220 station. As it is can be seen in Figure 9, there is practically no acceptance for elastically scattered protons in the RP220 station.

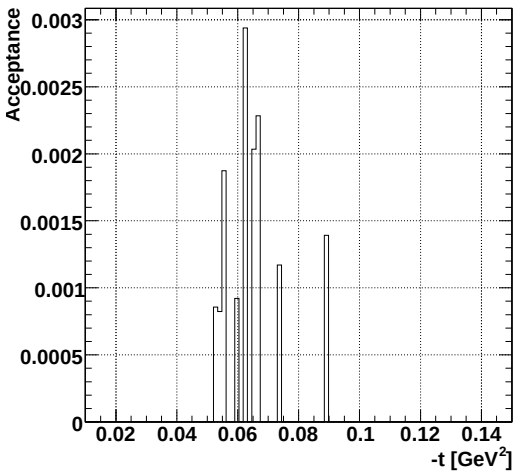

Figure 9: Acceptance of elastically scattered protons in the vertical RPs of the RP220 station.

3.2 Diffractive protons

The optical functions at the RP220 station also exhibit the dependence upon the proton momentum loss. Figure 10 shows the evolution of the magnification as a function of ξ. Also the effective lengths decrease with increasing $|\xi|$, which is shown in Figure 11. For

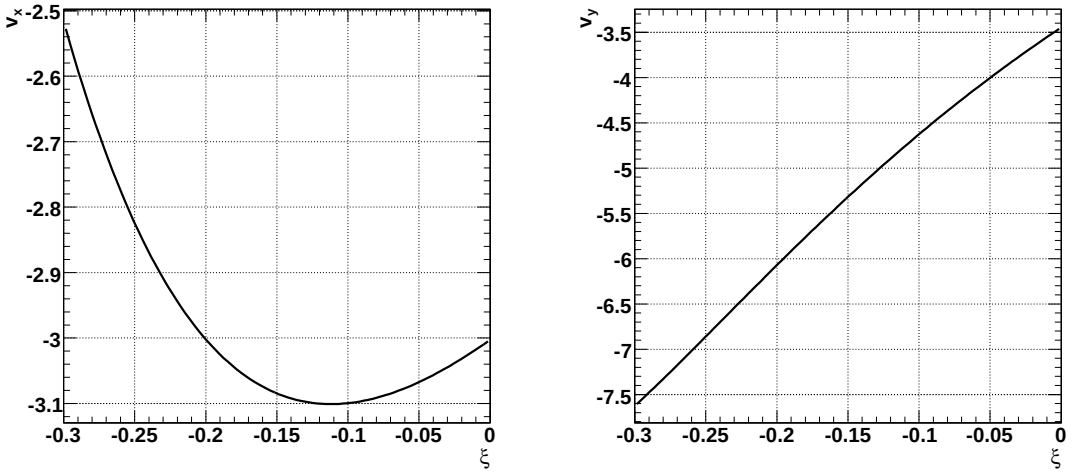

Figure 10: Magnification $v_x(\xi) = \partial x(s)/\partial x^*$ (left) and $v_y(\xi) = \partial y(s)/\partial y^*$ (right) at $s = 220\,\mathrm{m}$ from IP5 as a function of the fractional proton momentum loss ξ.

$\xi \approx -0.025$ and $\xi \approx -0.04$ they are equal to zero for horizontal and vertical projections, respectively. The fact that L_x and L_y reach the values of minus few tens of meters for higher fractional momentum losses allows for the detection of diffractive protons in the

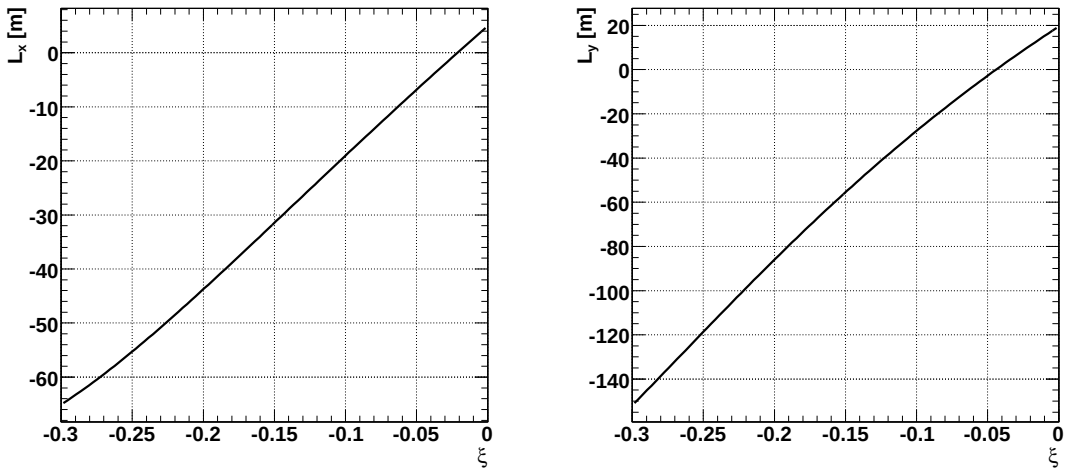

Figure 11: Effective lengths $L_x(\xi) = \partial x(s)/\partial\Theta_x^*$ (left) and $L_y(\xi) = \partial y(s)/\partial\Theta_y^*$ (right) at $s = 220\,\mathrm{m}$ from IP5 as a function of the fractional proton momentum loss ξ.

vertical RPs, as is presented in Figure 13 (right).

The evolution of the dispersion with respect to ξ is rather limited, as can be seen in Figure 12.

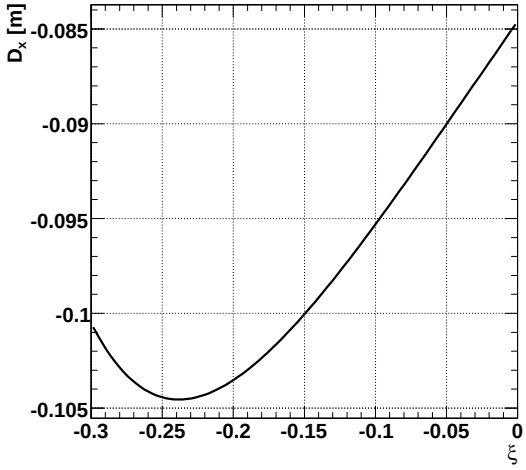

Figure 12: Dispersion $D_x(\xi) = \partial x(s)/\partial\xi$ at $s = 220\,\mathrm{m}$ from IP5 as a function of the fractional proton momentum loss ξ.

The acceptance for the diffractive protons at the RP220 station for 450 GeV optics with $\beta^* = 11\,\mathrm{m}$ is very limited. As it was already mentioned, the protons are lost in the machine apertures because of large beam sizes resulting from running at low energy. The surviving protons are mainly seen by the horizontal RPs (Figure 13, left) and also slightly by the vertical ones (right). The combined acceptance region, presented in Figure 14, is

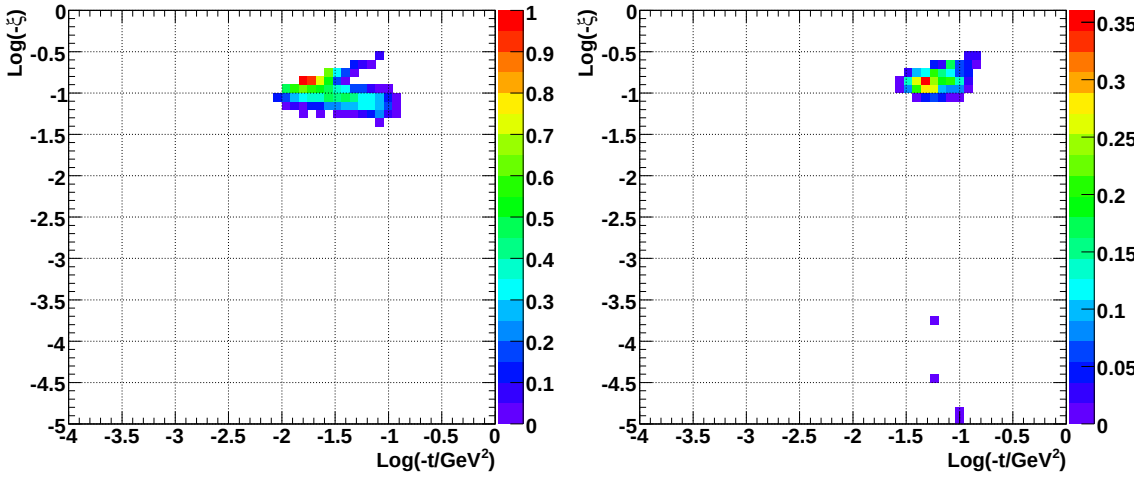

Figure 13: Acceptance in t and ξ for diffractively scattered protons in the RP220 station. Left: Horizontal RP. Right: Vertical RP.

approximately defined by $0.06 < -\xi < 0.25$ and $0.01\,\mathrm{GeV}^2 < -t < 0.1\,\mathrm{GeV}^2$. Due to large beams in RP220, the horizontal and vertical RPs do not overlap at all.

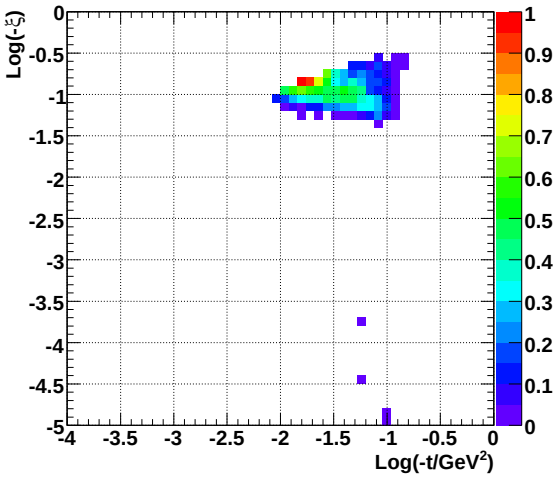

Figure 14: Combined acceptance in t and ξ for diffractively scattered protons in the RP220 station.

References

[1] TOTEM: Technical Design Report, CERN-LHCC-2004-002; addendum CERN-LHCC-2004-020.

[2] The TOTEM Collaboration, "The TOTEM Experiment at the LHC", 2008 JINST 3 S08007, doi: 10.1088/1748-0221/3/08/S08007.

[3] E. Wilson, "An Introduction to Particle Accelerators", Oxford University Press, 2006.

[4] V. Avati, K. Oesterberg, "Acceptance calculation methods for beta*=0.5 m optics", TOTEM-NOTE 2005-002, 2005.

[5] V. Avati, K. Oesterberg, "Optical function parametrization for beta*=1540 m optics", TOTEM-NOTE 2005-001, 2005.

[6] M. Deile, "Algebraic Determination of Roman Pot Acceptance and Resolution with the $\beta^* = 1540$ m Optics", TOTEM-NOTE 2006-002.

[7] The MAD-X Home Page, http://frs.home.cern.ch/frs/Xdoc/mad-X.html.

[8] http://proj-lhc-optics-web.web.cern.ch/proj-lhc-optics-web/V6.500/.

[9] H. Niewiadomski, "Reconstruction of Protons in the TOTEM Roman Pot Detectors at the LHC", Ph. D. Thesis, University of Manchester, United Kingdom, 2008.